Index

Paper 2.1

Qualification of Ultrasonic Flow Meters for Custody Transfer of Natural Gas Using Atmospheric Air Calibration Facilities

Jim Hill, GE Panametrics
Andreas Weber, RMG Messtechnik
Joern Weber, RMG Messtechnik

Qualification of Ultrasonic Flow Meters for Custody Transfer of Natural Gas Using Atmospheric Air Calibration Facilities

Jim Hill, GE Panametrics
Andreas Weber, RMG Messtechnik
Joern Weber, RMG Messtechnik

1 INTRODUCTION

The ability to operate in atmospheric air was a significant factor in the joint development by GE Panametrics and RMG Messtechnik of a custody transfer meter. Using air as a test medium yields major benefits. Two benefits are cost and availability. Natural gas calibration facilities cost thousands of dollars per day to use. This expense alone can accumulate into millions of dollars over the development of a meter, forming a barrier to entry to meter manufacturers. Also, the flow rate, if any, available at a natural gas test facility is dependent on seasonal, and even daily demand. The another factor is safety. Working at atmospheric pressure allows the developer to quickly make prototypes and design, without the safety concerns involved with high-pressure gas. Also, tests can be conducted with electronics exposed so that the performance of individual circuits and embedded software can be monitored, without the risk of encountering combustible gas. The final advantage is the flexibility that an open-loop calibration facility provides. Since the loop draws air from an open room, almost infinite combinations of installation conditions can be created. This is important, as actual field installations are a continuous distribution of configurations. Practical constraints limit the type of installations that can be simulated at a pressurized test facility.

Combined, these factors lead to the conclusion that air operation was not merely desirable but in fact essential in order for our companies to develop and qualify a high accuracy meter. The term *Qualification* is used in this paper differentiate between internal testing of product performance, and *Certification*, official performance testing by a regulating body. A clear distinction must be made between these terms and *Calibration*, which is the practice of reducing meter uncertainty by normalizing the meter to an accepted standard.

2 SIMILITUDE AND MODELING

The first step in the qualification process was to develop a model for the meter to extrapolate data from air testing to high-pressure natural gas and determine the limitations of air data. A dimensional analysis is used to identify the key dimensionless variables to scale the test results, and predict regions of similitude. An uncertainty analysis is also needed to identify which areas of uncertainty must be determined by experimental means.

2.1 Dimensional Analysis of a Multipath, Ultrasonic Flowmeter

The actual volumetric flow rate output by a ultrasonic meter with *m* paths is calculated by:

$$Q = \frac{\pi D}{4} \sum_{i=0}^{m} w_i \left(\frac{P_i^2 (T_u - T_d)_i}{2 L_i (T_u T_d)_i} \right). \quad (1)$$

See Section 6 for definitions of variables and terminology. Equation (1) can be restated as

$$Q = f(D, P, L, T_d, T_u). \quad (2)$$

This, in turn, can be combined with fluid properties and geometric factors such as inlet length, *l* , and rearranged into the standard form for a Buckingham PI analysis [1].

$$0 = f(Q, D, P, L, l, \rho, \mu, \beta, f) \tag{3}$$

Since there are 9 independent variables in equation 3, there should be 9-3 PI groups. (There are three unique variables: *mass, length*, and *time*). The performance of the meter can be modeled by maintaining similitude in the following six groups.

- Inlet Length $$I = l / D \tag{4}$$
- Cauchy Number $$C = \frac{V_{area}^2 \rho}{\beta} = M^2 \tag{5}$$
- Diametric Reynolds Number $$R_D = \frac{VD\rho}{\mu} \tag{6}$$
- Inlet Reynolds Number $$R_L = \frac{Vl\rho}{\mu} \tag{7}$$
- Transducer Angle $$\theta = \sin^{-1}\left(\frac{L}{P}\right) \tag{8}$$
- Acoustic Scale Factor $$ka = \frac{2\pi f D}{C} \tag{9}$$

In order to extrapolate calibration curves or correction factors, all of these dimensionless groups must be the same. In modeling, it is rarely possible to have similitude in more than two parameters. The experimental program must be organized remove the effect of the less significant parameters. For example, if inlet length, *l*, is 10, R_D dominates over R_L. However, to neglect the inlet Reynolds number, R_L, it must be above 100000. For a velocity of 0.5 m/s, this corresponds to a minimum straight run of 3 m in atmospheric air, 400 mm in 10 bar natural gas, and 200 mm in water. If this minimum length differs greatly with the inlet similitude, then velocity scaling may be used. A light turbulence mesh may also be used to speed boundary layer development, without effecting the character of the inlet flow field.

The angle at which the transducer is mounted in the meter body, like inlet length, is a mechanical feature, independent from fluid properties, and need not be considered in the comparison of performance. Natural gas typically has a velocity of sound 15% greater than air. This causes the acoustic scale factor to be smaller in natural gas. Data must be scaled accordingly, when estimating the effects of meter size and geometry.

This leaves only two dimensionless groups, the diametric Reynolds number and the Cauchy number to describe the behavior of the meter under different media. At this point it is important to examine what these groups actually represent. The Reynolds number is the relative magnitude of inertia forces to viscous forces acting on a differential volume. Likewise, the Cauchy number is the relative magnitude of inertia forces to elastic forces acting on the same differential volume. One method of analyzing a complicated system is the use of force ratios [2]. To place the force ratios on a common frame of reference, we scale the viscous force ratio relative to the laminar transition point ($\boldsymbol{R_D}$ = 6000). The elastic force ratio is scaled relative to the limit for incompressible flow ($\boldsymbol{M}$ = 0.3).

- Scaled Viscous Force Ratio $$FR_v = \frac{6000}{R_D} \tag{10}$$

- Scaled Elastic Force Ratio $$FR_E = \frac{M^2}{0.3^2} \tag{11}$$

Figure 1 is a plot of the two, scaled force-ratios as a function of velocity. Graph *a)* represents air at 0 bar, while *b*) represents natural gas at 20bar. Examining the chart shows that under

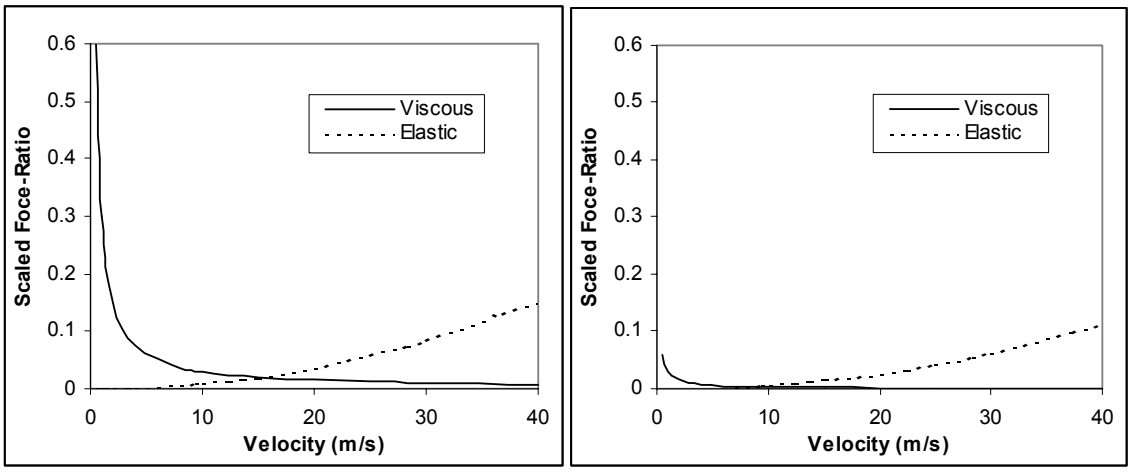

Fig. 1 – Viscous and Elastic Force Ratios for *a)* Air and *b)* Natural Gas

high-pressure natural gas, the performance of the meter is controlled strictly by inertial forces up to a velocity of 25 m/s.

2.2 Uncertainty Analysis of a Multipath, Ultrasonic Flowmeter

The following analysis only accounts for the uncertainty in the actual volumetric output, *Q*, of the flow meter. It does not account for uncertainty in converting the actual volumetric flow to normal, mass, or energy flow rates. Again, the actual flow rate is given by (1). The propagated uncertainty in flow measurement due to the uncertainty in the m^{th} parameter in path *i* is [3]:

$$\xi_Q = \sqrt{\sum_{i=1}^{I}\sum_{m=1}^{M}\left(w_i \xi_{i,m} \frac{\partial Q}{\partial \Phi_{i,m}}\right)^2}. \tag{12}$$

where w_i is the weighting factor of the individual path of a multipath meter. One way to look at the propagation of error is to calculate the propagation factor, Ψ, for each parameter,Φ. The normalized uncertainty of the flow measurement due to the uncertainly in each parameter is:

$$\frac{\xi_{q_m}}{Q} = \Psi_m \frac{\xi_m}{\Phi_m}. \tag{13}$$

where the propagation factor, ψ, is defined as:

$$\Psi_m = \frac{1}{\Phi_m}\frac{\partial Q}{\partial \Phi_m}. \qquad (14)$$

Table 1 catalogs the propagation factor for each parameter and the amount of uncertainty budgeted to each parameter in the design of the USZ-08 meter.

Table 1 – Error Budget and Propagation Factors for Meter Parameters

Parameter	Error Budget %	Propagation Factor	Allowable Uncertainty
Path Length	0.1	2	0.2 mm
Axial Length	0.1	-1	0.2 mm
Internal Diameter	0.05	2	0.07 mm
Transit Time	0.2	-2	1.0 μs
Differential Transit Time	0.1	1	0.02 μs
Weighting Factor	0.2	1	0.002

It is important to note that the value budgeted is the total uncertainty for that parameter. For example, the uncertainty in geometric parameters must also include the dimensional effects of pressure and temperature changes. These uncertainties must be limited by active compensation to account for pressure and temperature [4], or the mechanical design of both the meter body and transducer mounting system must be sufficiently rigid to keep distortion negligible.

3 EFFECT OF INSTALLATION ON MEASUREMENT UNCERTAINTY

The uncertainty in geometric parameters can be verified by direct mechanical measurement. Uncertainty in time resolution and electronic delays likewise can be determined by static and dynamic measurements of sound speed in fluids of known composition and state properties. The uncertainty in the weighting factor is much more difficult to ascertain. The weighting factor is the fractional amount of velocity measured for each path of the multipath meter that is used to calculate the area average velocity. The uncertainty in this component depends on the assumptions made in calculating the weighting factors, and the actual velocity vector field existing in the meter section.

3.1 Gaussian Quadrature Integration

The GE Panametrics / RMG ultrasonic flowmeter product line uses the principle of Gaussian quadrature integration, specifically Chebyshev quadrature [5], to calculate weighting factors and abscissa locations for each path. Figure 1 depicts a meter body with interrogation paths located in the y-z plane. While in practical use the ultrasonic ports are installed in horizontal planes to prevent collection of sediment or condensate, the planes have been rotated 90° to keep the notation consistent with standard mathematical references.

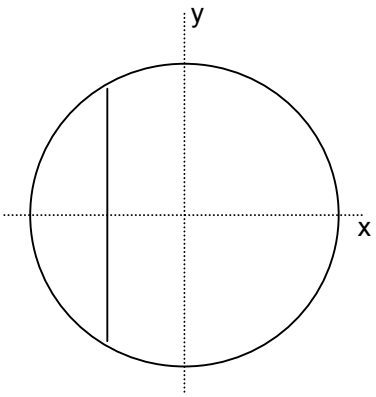

Fig. 1 - Projection of Ultrasonic Beam Path

The first step in applying quadrature integration is to design the three-dimensional system such that it can be described by this one-dimensional formula. This is achieved by keeping the axial length of the measurement system as short as possible so that the velocity field is independent of axial position. The effect of secondary flows (velocity components perpendicular to the pipe axis) are eliminated by using pairs of crossed interrogation paths, or by reflecting the ultrasonic beam back in the identical *y*-plane. The line

average velocity in y-plane for any given point on the x-axis, $V_l(x)$, is:

$$V_L(x) = \frac{1}{2\sqrt{1-x^2}} \int_{-\sqrt{1-x^2}}^{\sqrt{1-x^2}} v_z(x,y)dy. \tag{15}$$

With the line velocity in this form, the error in using quadrature integration can be expressed as:

$$E = \int_{-D/2}^{D/2} V_L(x)dx - \sum_i^m w_i V_L(x_i)\,. \tag{16}$$

Hildebrand [5] offers explicit solution for E when the line integral is of a closed form. Otherwise, (16) may be solved by numerical methods.

The distribution of axial velocities can be obtained from experimental data and computational fluid dynamics [6] for specific installations disturbances. However, a general model that describes a spectrum of flow fields is desirable for a robust uncertainty analysis. Flow is too chaotic to solve explicitly for the vector field. However, the shear stress, τ, at any point (*x, y*) must be related to the turbulence magnitude $\nu_x\nu_y$, and the viscosity, μ, by the relationship[7]:

$$\tau = -\mu\frac{dv}{dr} - \rho\overline{\upsilon_x\upsilon_y}\,. \tag{17}$$

It is shown in [8] that the turbulent stress dominates the flow except at the pipe wall and the point of maximum velocity, which is usually the center of the pipe. The standard solution to this boundary value problem neglects the viscous forces, yielding:

$$\frac{v_m - v}{v_*} = 2.5\ln\left(\frac{1-R}{R}\right). \tag{18}$$

where v_* is the friction velocity. This expression has two drawbacks. It is not defined for points near the pipe wall, requiring an estimate of the boundary layer thickness. It also has a discontinuity in the second derivative of the velocity at the point of maximum flow. Blasius[9] offers a simpler formulation that accurately depicts(18) for Reynolds numbers above 25000 with a single equation:

$$\frac{v}{v_m} = \left(\frac{R-r}{R}\right)^b. \tag{19}$$

This form is not a unique solution to (17) and also has a slope discontinuity. However, these problems can be overcome by allowing a linear combination of these functions. If the point of maximum velocity is not assumed to be at *x*=0, but instead at an arbitrary X_n, then the distribution of the axial velocity component can be expressed as the summation of *N* functions:

$$v_z(x,y) = \sum_{n=0}^{N} A_n \left(1 - \frac{2\left((x-X_n)^2 + y^2\right)^{1/2}}{\left(R^2 - x^2 + (x-X_n)^2\right)^{1/2} + \left(y^2 + \left(\sqrt{R^2-y^2} - X_n\right)^2\right)}\right)^{b_n}. \tag{20}$$

This only expresses asymmetry of the flow field along the x-axis. Equation (20) can be expanded to have the maximum velocity at any point in the plane. However, this can also be handled by coordinate rotation during computation. The advantage of the series model is that each term can be evaluated independently by (15) and (16). The total uncertainty is taken as

the RMS of the uncertainty for each mode, weighted by the amplitude in a similar fashion as (12). Because of this, the maximum uncertainty of any combination modes will be approximately the maximum uncertainty of the worst case combination.

A software program was used to apply (20) to (15) and (16), continually varying *X, b*, and the axis orientation. For three-plane Chebyshev quadrature, the uncertainty in weighting factor stayed under 0.2% for all combinations where $0.01<b<0.15$ and $-0.25R<X<0.25R$. The next step was to experimentally determine what profiles exist behind an array of flow disturbances.

3.2 Flow Fields Generated by Standard Installations

The ability to make accurate measurements in atmospheric air was critical to the development program at this point. In addition to the profile shape and asymmetry, we also wanted to measure the secondary flow patterns. Figure 2 depicts the elements of the flow field that we wanted to quantify for standard installation conditions. The details of the flow were

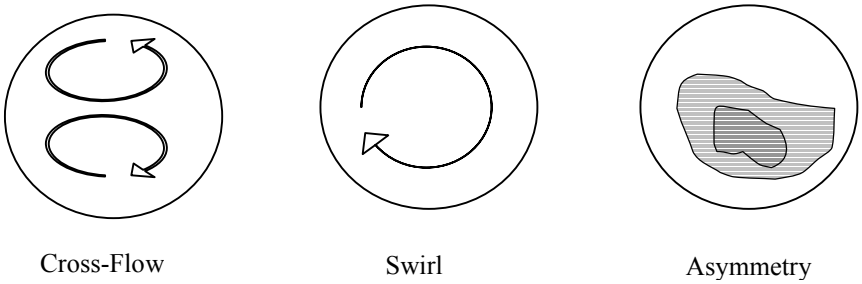

Fig. 2 - Types of Disturbed Flow

measured by using the features of the USZ-08-6P meter. The meter uses a three-plane Gauss/Chebyshev configuration. The crossed paths measure the secondary flow in the plane as well as the axial flow component (Fig. 3).

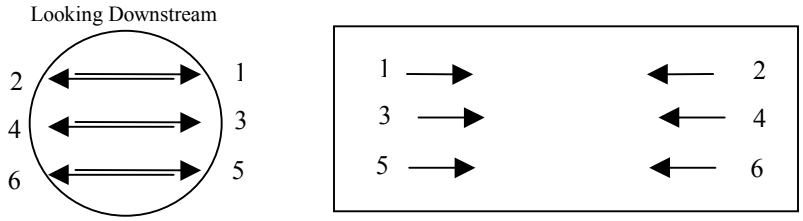

Fig. 3 - Layout of Paths Used in the USZ-08-6P Flowmeter.

Six installation conditions were tested and compared to the standard installation of ten diameters of straight run. The inlet length was increased to 20D to see if increased profile development had any effect. The inlet length was returned to 10D and the following inlet conditions were attached:

- Single Elbow In-Plane with Meter
- Single Elbow 90° from Meter Plane
- Double Out-of-Plane Elbows
- Double Out-of-Plane Elbows with a Half-Moon Plate Between the Elbows

Figure 4 depicts the Blasius factor of the primary profile mode. A large factor results in a more bullet shaped the profile. Small numbers indicate a flat profile. The greater the level of disturbance, the faster the factor drops down to an asymptotic level. This makes sense if we examine equation (17). These disturbances create excess turbulence and vorticity, increasing the shear at the wall and likewise the slope of the profile at the wall. Except for three points in the low Reynolds numbers, the measured factors stayed within the limits mandated by the uncertainty budget for three-plane Chebyshev quadrature.

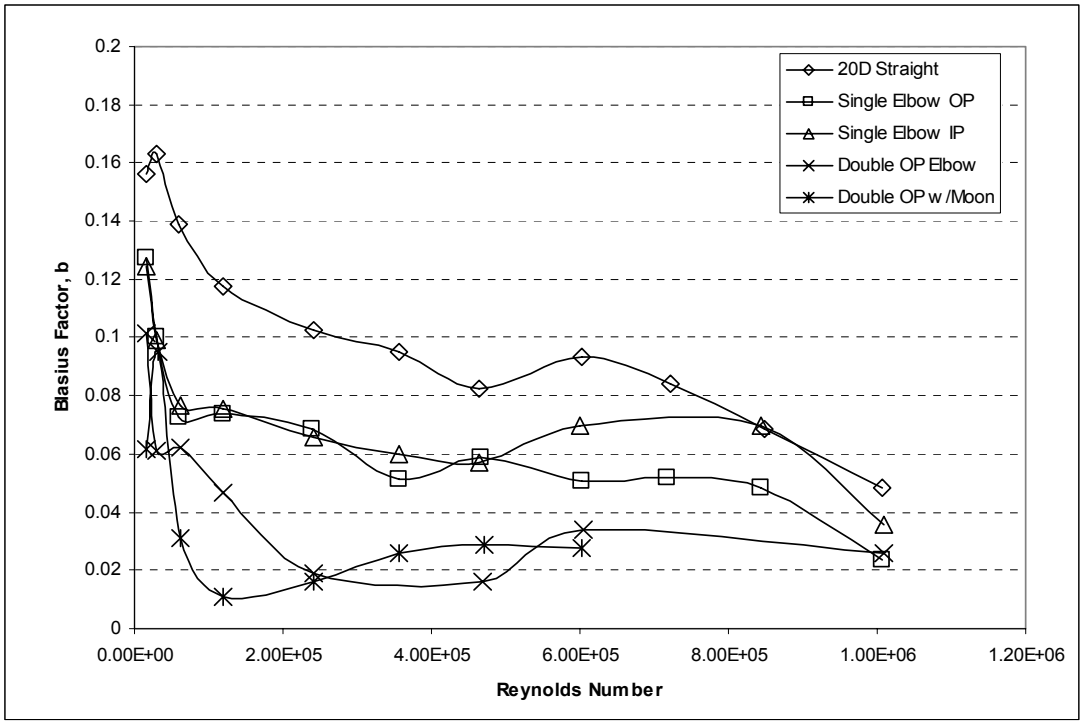

Fig. 4 - Blasius Profile Factor for Five Standard Meter Installations

The asymmetry also stayed within the prescribed limits (Fig. 5). It is interesting to note that the worst asymmetry was observed behind the 20D straight inlet at low velocities. This indicates that profiles may not develop properly even with significant straight run unless there is some feature to "trip" turbulent behavior.

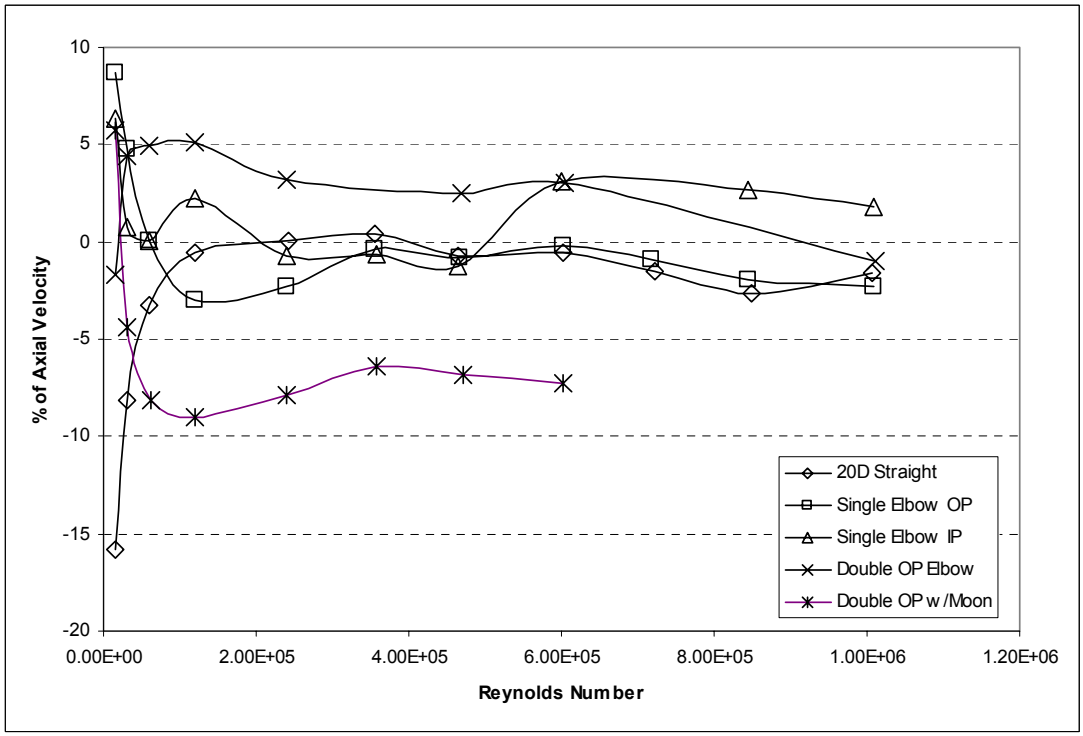

Fig. 5 – Asymmetry of the Flow Profile for Five Standard Meter Installations

Figures 6 and 7 display the levels of secondary flows generated by the different disturbances. The high-level disturbance (double elbows separated by a half-plate) generates secondary flow three times greater than the double elbows alone.

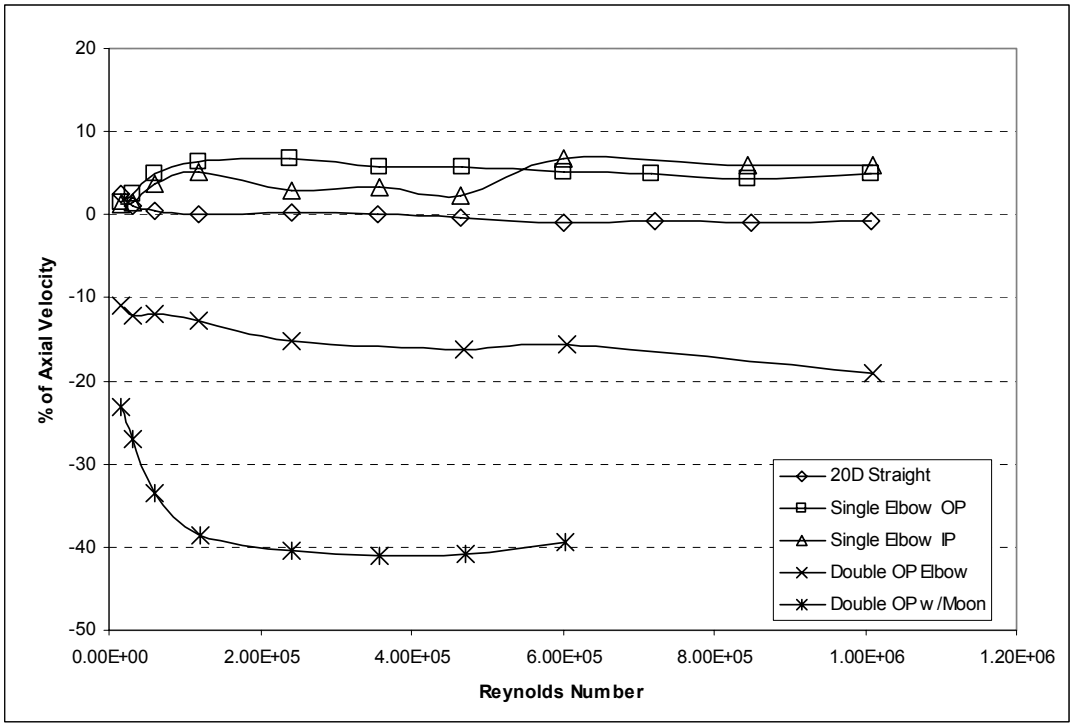

Fig. 6 – Swirl Generated by Five Standard Meter Installations

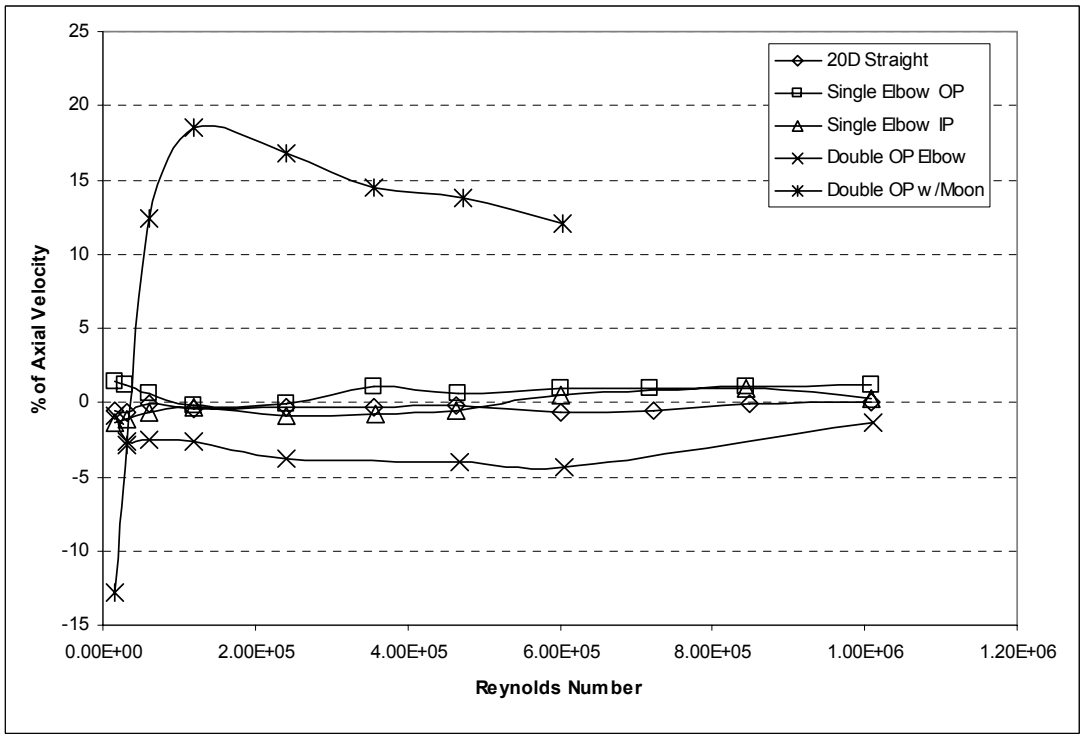

Fig. 7 – Cross-Flow Generated by Five Standard Meter Installations

The error shifts generated by these distorted profiles was under 0.5% for all but the lowest Reynolds numbers. This was outside our budgeted uncertainty but close enough to give us confidence that the meter would have uncertainties due to installation of under 0.3% when the meter was tested with high pressure natural gas. At 10 bar of methane, the level of disturbance decreases with increased Reynolds number and the ultrasonic signal would be an order of magnitude stronger compared to atmospheric pressure air, allowing for better timing accuracy.

4 UNCERTAINTY DUE TO VARIATION OF FLUID PROPERTIES

The last step was to confirm that tests in natural gas would go as predicted from the air tests and the model previously developed. To verify this, the installation effect tests were repeated in 10 bar natural gas[10] (Fig. 8). As predicted, the stability and accuracy of the instrument improved with the denser fluid. It showed that the air testing was a worst case situation.

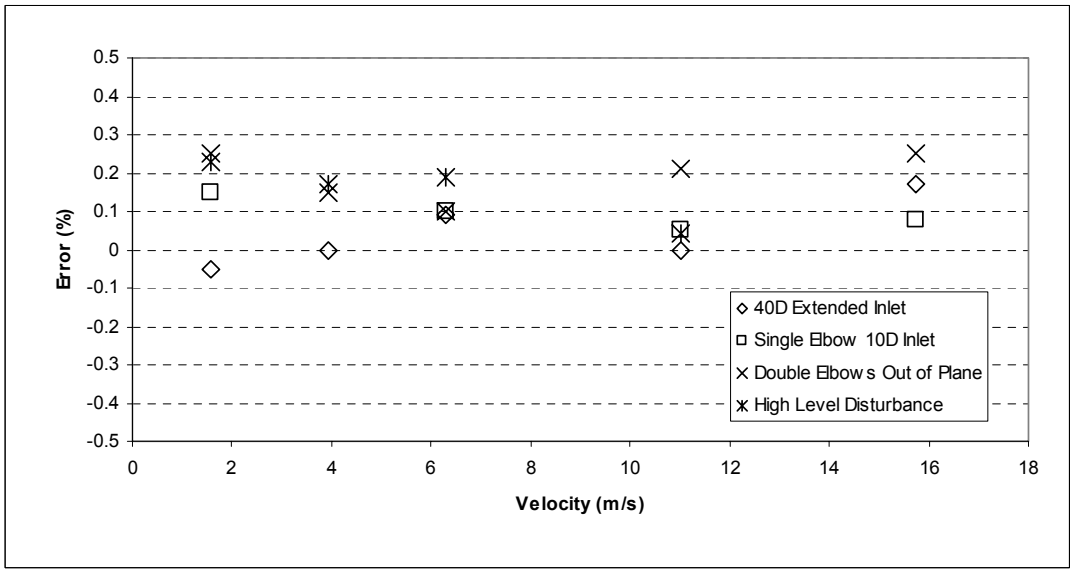

Fig. 8 – Error Shifts for Four Installations in 10 bar Natural Gas

The next step was to compare calibrations performed at atmospheric air with those under high-pressure natural gas. Figure 9 is the calibration of a 200mm, ANSI600, meter. This size is the smallest meter available in the six-path configuration. The effect of low Reynolds numbers can be seen in the air testing. At higher velocities, the measurements agree within 0.2%. This meter used no active compensation for pressure and temperature, depending on a reinforced design to keep the geometry stable under the stress. Larger meters show less effects due viscous forces (Fig. 10 and Fig. 11).

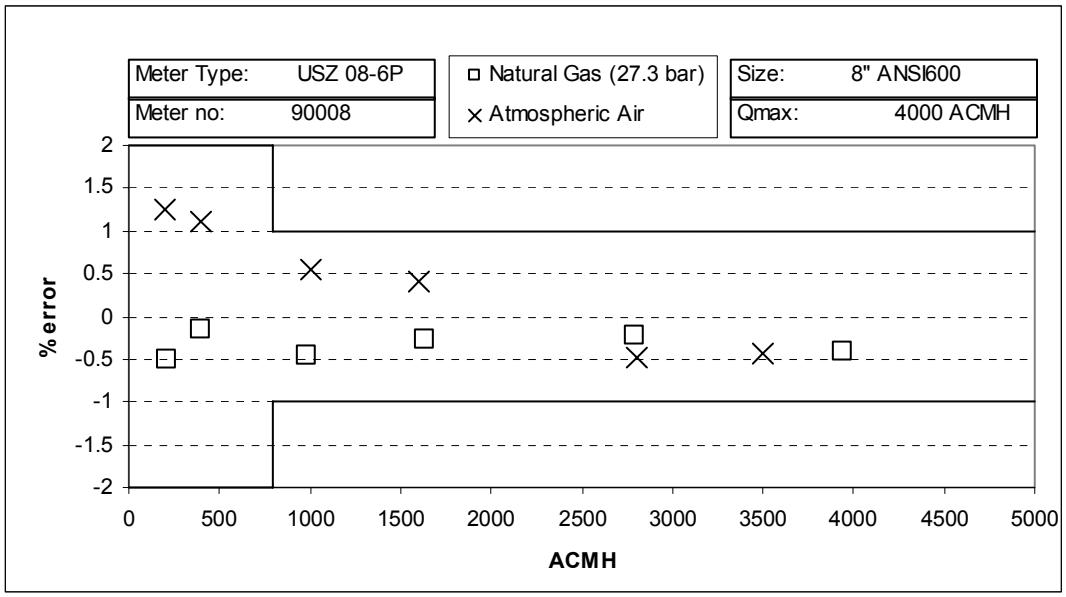

Fig. 9 – Comparison between Air and Natural Gas Calibration in 8 inch size

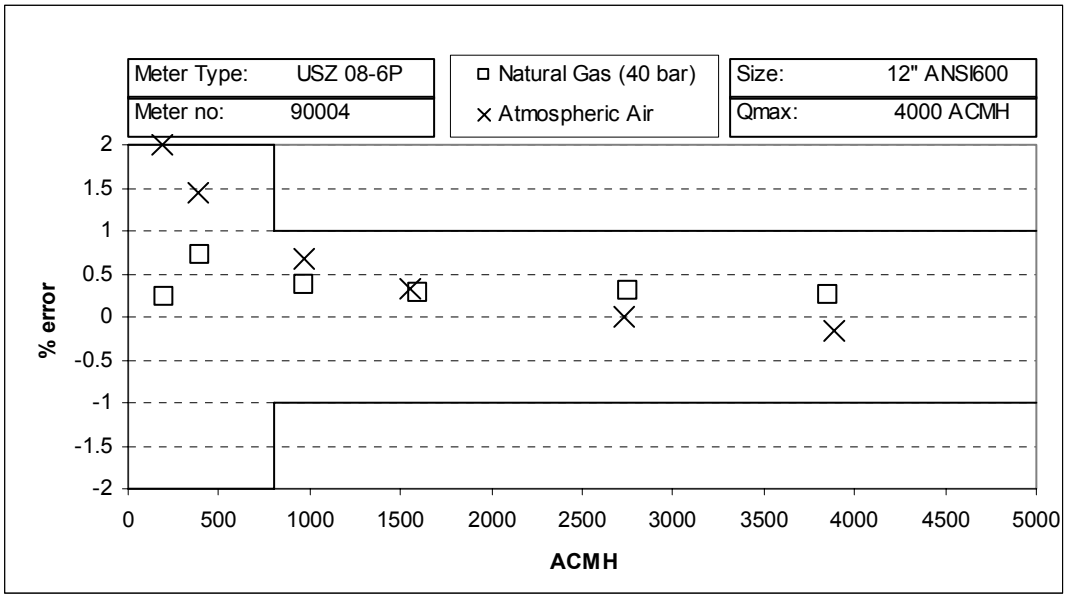

Fig. 10 – Comparison between Air and Natural Gas Calibration of 12 Inch Meter

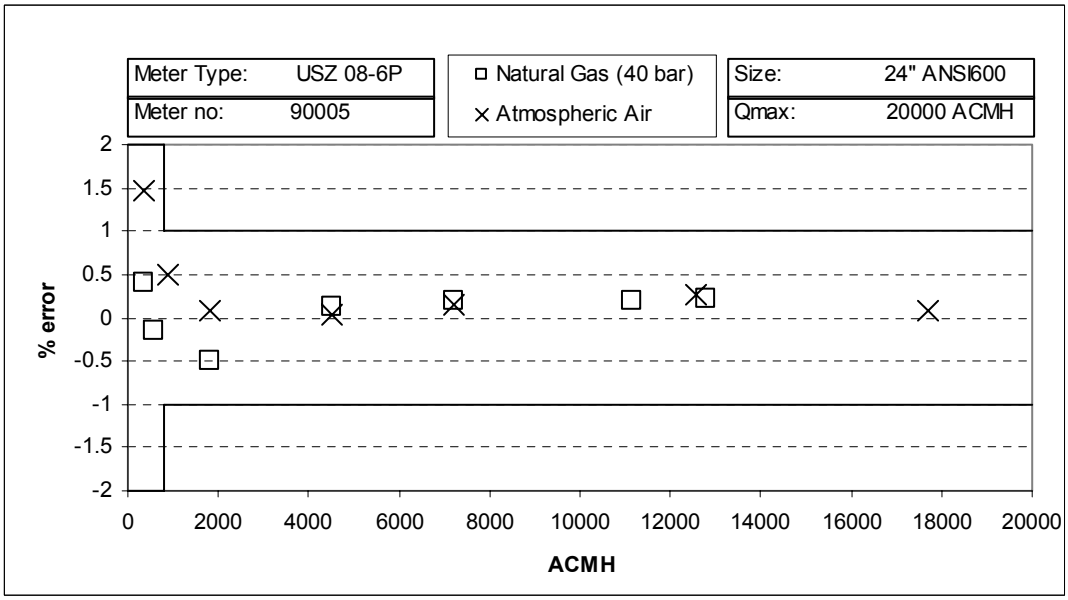

Fig. 11 – Comparison between Air and Natural Gas Calibration of 24 Inch Meter

5 CONCLUSION

Without the ability to measure flow accurately at atmospheric pressure, it is unlikely that this metering technology could have been developed without external help from a public agency or distribution concern. Even with low-pressure operation, the project was heavily dependent on computational physics not only for the fluid dynamics, but the acoustics and digital signal processing that completes the meter.

Such modeling will become more important in the future, as standards are developed to use air as a calibration medium. As large ultrasonic meters outgrow all measurement facilities, a solid understanding of the principles will be required in order to use meters without calibration. Presently, low-pressure air calibration is only advisable in large pipe sizes where Reynolds mismatch can be minimized. The uncertainty analysis does show that it is possible to build meters with flow-weighted, mean uncertainties less than 0.4% without calibration, if

installation guidelines are observed. Where we go from here, depends on how the natural gas international community deals with the definition and measurement of uncertainty, absolute or relative, and how this uncertainty propagates out to actual energy based unaccountables at the final point of delivery.

6 NOTATION

A_n Modal Amplitude of a Flow Profile Series Element
b Shape Factor of a Flow Profile Series Element
C Cauchy Number. Equivilant to the Square of the Mach Number
D Inside Diameter of the Flow Meter
E Quadrature Integration Error Associated with a Specific Functional Form
f Transmission Frequency of a Ultrasonic Flow Meter
FR_v Viscous Force Ratio Scaled Relative to Onset of Laminar Flow
FR_E Elastic Force Ratio Scaled Relative to Onset of Compressive Flow
I Normalized Inlet Length, Express in Number of Diameters
kD Acoustic Scale Factor, Product of the Wave Number and Meter Diameter
l Actual Inlet Length of the Ultrasonic Meter
L Length of the Axial Projection of the Ultrasonic Beam Path
M Mach Number, Ratio of the Fluid Velocity to Velocity of Sound
P Length of the Ultrasonic Beam Path in the Fluid
Q Actual Volumetric Flow Rate
R Inside Radius of a Pipe
R_D Diametric Reynolds Number
R_L Inlet Reynolds Number
T_d Transit Time of an Ultrasonic Pulse Traveling Downstream
T_d Transit Time of an Ultrasonic Pulse Traveling Upstream
V_L Average Velocity Along the Ultrasonic Beam Path
w Integration Weighting Factor
X Asymmetry Factor, Expressed in % of Pipe Radius
β Adiabatic Bulk Modulus of Fluid
ξ Uncertainty
μ Dynamic Viscosity
ρ Density of Fluid
$\upsilon_x\upsilon_y$ Turbulence Product
Φ Independent Parameter in a Equation
Ψ Uncertainty Propagation Factor
θ Angle Between the Ultrasonic Beam and a Vector Normal to Meter Axis

7 ACKNOWLEDGMENT

The authors would like to acknowledge GE Panametrics and RMG Messtechnik for permission to publish this paper which is excerpted from Ultrasonic Report UR-271, ©2002 by Panametrics, Inc. The authors would also like to thank Larry Lynnworth for his insight and advice in the preparation of this manuscript. Special thanks are due David Chleck, Hans Kastner, and Tom Nicholson whose vision, drive, and support made this development project possible.

8 REFERENCES

[1] D. ZWILLINGER. *Standard Mathematical Tables and Formulae*, 30th Edition, CRC Press, New York, 1996 p. 733

[2] L. MALVERN, *Introduction to the Mechanics of a Continuous Medium*, Prentice-Hall, Englewood Cliffs, 1969 pp. 471-474

[3] B. TAYLOR and C. KUYATT, *Guidelines for Evaluating and Expressing the Uncertainty of NIST Measurement Results*, Technical Note 1297, NIST, 1994

[4] *Measurement of Gas by Multipath Ultrasonic Meters*, Report No. 9, AGA, 1998

[5] F. HILDEBRAND, *Introduction to Numerical Analysis*, Dover, New York, 1974 pp. 379-432

[6] A. HILGENSTOCK, T. HÜWENER, B. NATH, *Prediction of Measurement Errors of Ultrasonic Flowmeters in Disturbed Flow Conditions*, GERG II, 2000

[7] R. STREET, *Elementary Fluid Mechanics*, Wiley, New York, 1996 pp. 329-331

[8] J. LAUFER, N.A.C.A. Report 1174, 1954

[9] H. BLASIUS, *Forschungsarbeiten auf dem Gebiete des Ingenieurwesens*, 131, 1913

[10] J. WALTERS, X. AO, J. HILL, L. LYNNWORTH, *Transit-Time Ultrasonic Flowmeters*, Proc. 41st Annual CGA Gas Measurement, 2002.